N91-22337

DEVELOPMENT AND TESTING OF CONTROLLER PERFORMANCE EVALUATION METHODOLOGY FOR MULTI-INPUT/MULTI-OUTPUT DIGITAL CONTROL SYSTEMS

Anthony Pototzky*, Carol Wieseman†§, Sherwood Tiffany Hoadley† and Vivek Mukhopadhyay†

Fourth Workshop on the Computational Control of Flexible Aerospace Systems

Williamsburg, Virginia

July 11-13, 1990

*Lockheed Engineering and Sciences Company †NASA Langley Research Center §Presenter

OUTLINE

- Motivation
- Objectives of CPE
- CPE Computations
- CPE Implementation
- Wind-Tunnel Test Results
- Concluding Remarks

MOTIVATION

Active controls are becoming an increasingly important means to enhance the performance of aircraft. But, because the process of designing some of the multi-input/multi-output (MIMO) digital control laws uses relatively untested theoretical methods, it has become crucial to validate the design methodology through experimentation. For classical single-input/single-output (SISO) control systems, analysis tools such as Nyquist diagrams were developed and used to determine the stability and robustness of the closed-loop system. For MIMO systems, Nyquist techniques are inadequate. However, analytical methods based on the use of singular values of return-difference matrices at various points in the control loop have been developed recently (references 1 - 3) to examine the stability and robustness of the MIMO closed-loop system.

Flutter testing of aeroelastic wind-tunnel models is, in general, a risky endeavor because the onset of flutter cannot be predicted precisely using even the most sophisticated analysis tools available. Closed-loop flutter suppression testing adds an extra risk because the controller itself can potentially destabilize the model. To reduce these risks, on-line near real-time controller-performance-evaluation (CPE) methods were developed to assess the stability and the robustness of MIMO flutter suppression systems.

This presentation describes the development and implementation of this CPE capability and briefly discusses the structure of the data flow, the signal processing methods used to process the data, and the software developed to generate the transfer functions. This methodology is generic in nature and can be used in any type of MIMO digital controller application including digital flight control systems, digitally-controlled spacecraft structures, and actively controlled wind-tunnel models. Results of applying the CPE methodology to evaluate (in near real-time) MIMO digital flutter suppression systems being tested on the Rockwell Active Flexible Wing (AFW) wind-tunnel model (reference 4) are presented to demonstrate the CPE capability. The AFW wind-tunnel test program is described in references 5 and 6.

MOTIVATION

- Active controls becoming increasingly important means to enhance aircraft performance
- Validation of control law design methodology
- CPE method to evaluate performance of MIMO digital controllers
  - Stability
  - Robustness
- Reduce risk of flutter suppression testing
- Demonstrate CPE method during FSS tests on AFW

OBJECTIVES OF CPE

Simplified block diagrams of the basic control problems are presented in the figure. The plant to be controlled is represented mathematically by a frequency domain transfer matrix, **G**, with outputs, y, and inputs, e. The controller is represented mathematically by a transfer matrix, **H**, with inputs, y, and outputs, x. An external excitation, u, is used to excite the system in a specified fashion. This excitation is used to compute transfer functions between outputs and inputs in either open- or closed-loop systems. The open-loop system is one in which the control law outputs (commands required for controlling plant response) are not fed back into the system; i.e., the switch depicted in the figure on the left is open.

Controller performance is evaluated both open and closed loop. The process is outlined conceptually for the flutter suppression system application as follows:

Open-loop

Step 1: Verify the controller, **H**, by comparing the computed transfer functions with transfer functions supplied by control law designers.

Step 2: Predict closed-loop stability based on open-loop information to determine whether the control law will stabilize or destabilize the system when the loop is closed.

Closed-loop

Step 1: Determine the stability margins of the closed-loop system during the closed-loop testing.

Step 2: Determine open-loop plant stability during the closed-loop testing to determine the open-loop flutter boundary.

OBJECTIVES OF CPE

Open Loop

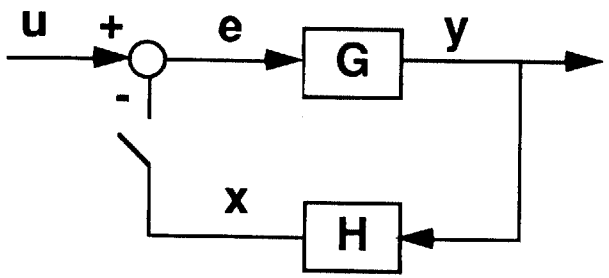

1) Verify controller
2) Predict closed-loop system stability

Closed Loop

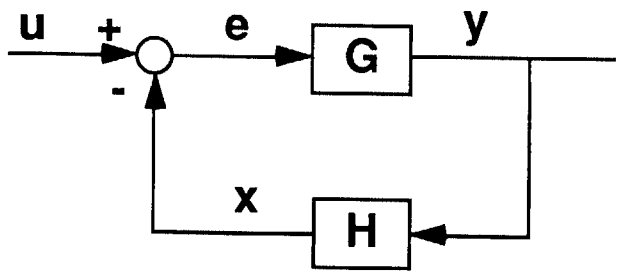

1) Calculate closed-loop stability margins
2) Determine open-loop plant stability

FLOWCHART OF CPE PROCEDURES

This figure shows a flowchart which outlines the CPE procedures and identifies the calculations involved. This figure will serve as an outline for a description of the CPE methodology.

Two basic tasks are involved. The first involves converting the time history data to the frequency domain and computing transfer functions of each plant response and controller output to the excitation and then combining them to form the transfer matrices. The second task involves using the transfer matrices to determine the plant and controller transfer matrices, to obtain the return difference matrices and their singular values, and to calculate determinants and eigenvalues to meet the objectives that were stated previously.

The calculation of the transfer functions is described in more detail in the next figure.

FLOWCHART OF CPE PROCEDURES

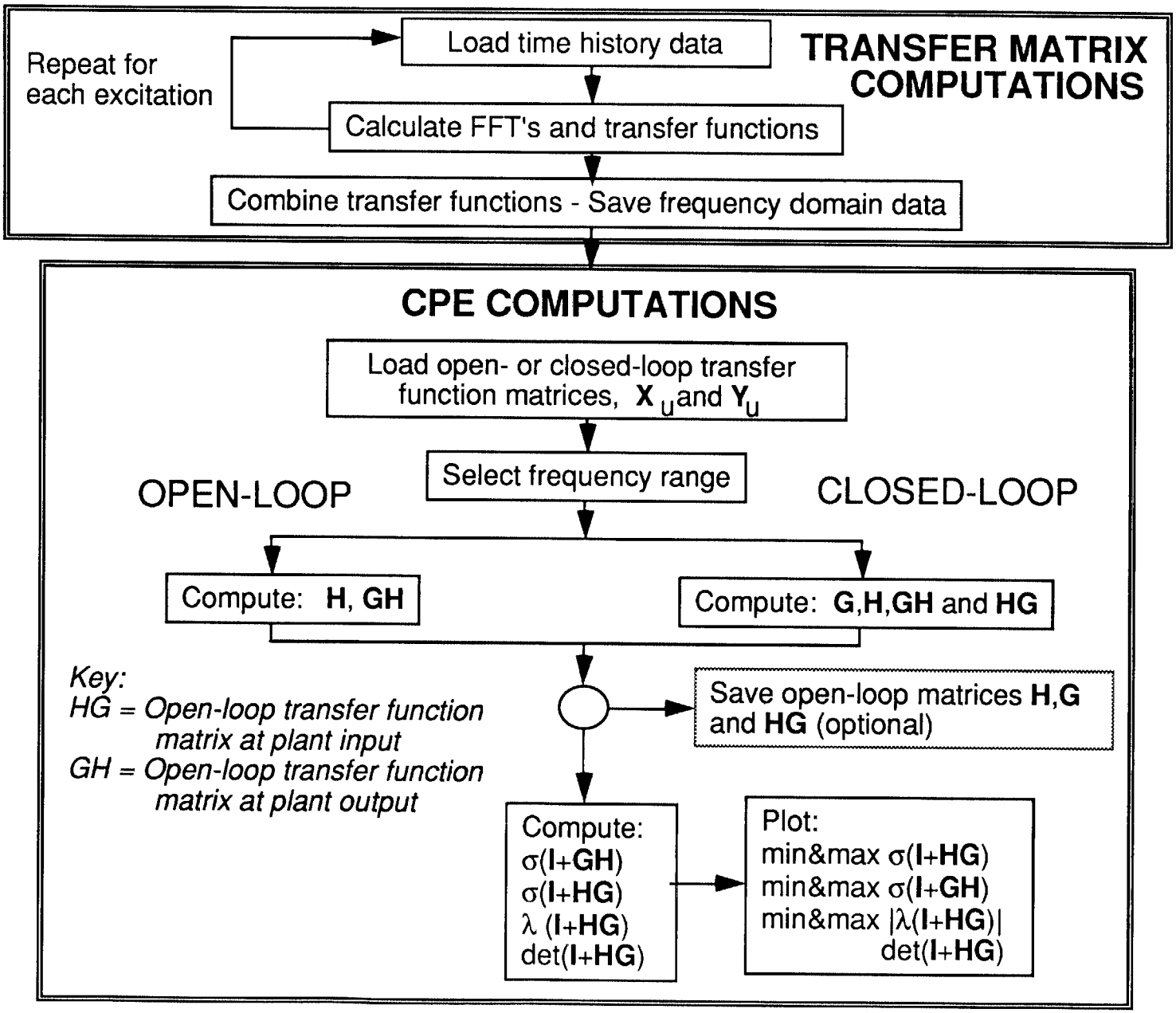

TRANSFER FUNCTION CALCULATION

The first step in computing transfer functions **G** and **H** is to acquire time histories of excitations, u, and responses, x and y. The first and last five seconds of an example time history of an excitation and a typical response are shown in the figure. The input excitation to perform CPE was a constant amplitude logarithmic sine sweep with a ramp-in and ramp-out. The initial frequency was 5 Hz and the final frequency was typically 35 Hz. The duration of the excitation is approximately 150 seconds. The data was saved at a 200 Hz sampling rate. The sample rate and low quantization levels explains the jaggedness in the time history plots.

Because of the long time history and large number of data points, overlap averaging was performed. The overlap-averaging capability allows long time histories to be partitioned into shorter time spans, taking advantage of long periods of time history data to average out noise. In addition, a zero-fill capability was available to zero-fill time history data to an exact increment of a power of two needed for FFT computations. The overlap-averaging capability with zero-fill provided optimum use of the time history data which were obtained. The size of the time-history partition as well as the amount of overlap were options which could be chosen.

The next step in computing transfer functions is to employ Fast Fourier Transform (FFT) techniques and overlap averaging. The FFT's of the excitation and each response are computed and from the FFT's the appropriate power spectra and cross spectra are constructed. The transfer functions are then calculated from the ratio of the averaged cross spectrum at some output resulting from the excitation to the averaged power spectrum of the excitation. The equations used in the computation of the transfer function at the controller output, X_u, and at the plant output, Y_u, are shown in the bottom of the figure. N is the number of overlap components making up the averaged spectrum.

The method was extended in the present study to include additional data-windowing capabilities. Windowing capabilities include ramp-in/ramp-out, Hanning, cosine taper, and cosine bell. Hanning windows were used during the flutter suppression testing.

TRANSFER FUNCTION CALCULATION

Time Domain

Excitation, u

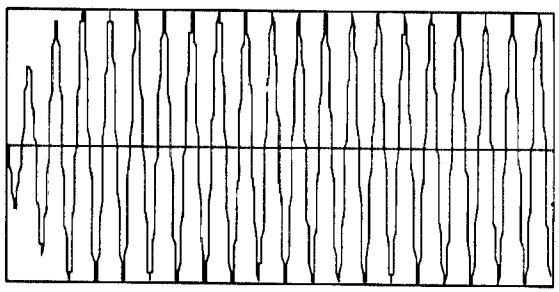

...

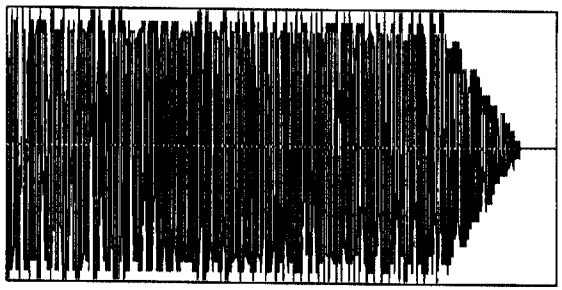

Response, y or x

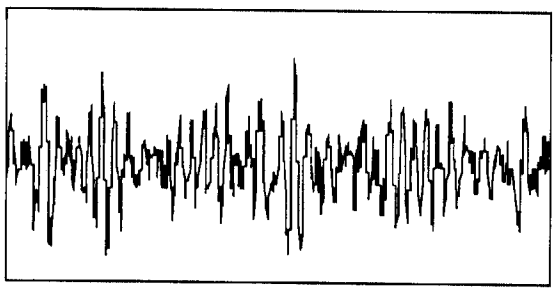

...

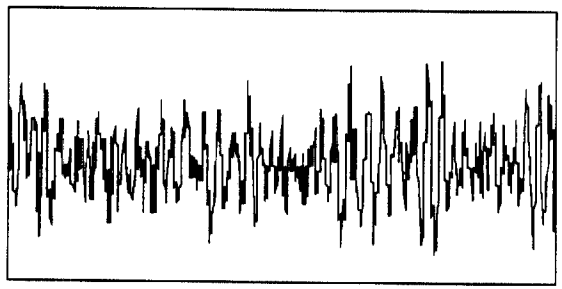

Frequency Domain

$$(X_u)_{ij} = \frac{\sum_{m=1}^{N} \left(S_{u_i x_j}\right)_m}{\sum_{m=1}^{N} \left(S_{u_j u_i}\right)_m}$$

$$(Y_u)_{ij} = \frac{\sum_{m=1}^{N} \left(S_{u_i y_j}\right)_m}{\sum_{m=1}^{N} \left(S_{u_j u_i}\right)_m}$$

TRANSFER MATRIX FORMATION

This figure shows how the transfer matrices are constructed from the transfer functions for a two by two controller. Each input to **G** represents a pair of control surfaces; each output from **G** represents a pair of accelerometers.

The first pair of control surfaces is excited with a sine-sweep excitation, u_1, and the transfer functions of each plant response, y_1 and y_2, and each controller output, x_1 and x_2, with respect to the excitation, u_1, are calculated. The transfer functions of the plant outputs to the first excitation make up the first column of the plant-output transfer matrix, $\mathbf{Y_u}$, shown in the upper right of the figure. The transfer functions of the controller outputs to the first excitation make up the first column of the controller-output transfer matrix, $\mathbf{X_u}$, shown in the bottom right of the figure.

The second pair of control surfaces is excited with a sine-sweep excitation, u_2, and the transfer functions of each plant response, y_1 and y_2, and each controller output, x_1 and x_2, with respect to the excitation, u_2, are calculated. The second column contains the transfer functions of the outputs with respect to the second excitation.

The two matrices, $\mathbf{X_u}$ and $\mathbf{Y_u}$, form the basis of all the remaining CPE calculations.

TRANSFER MATRIX FORMATION

FOR 2X2 CONTROLLER

Time Domain | **Frequency Domain**

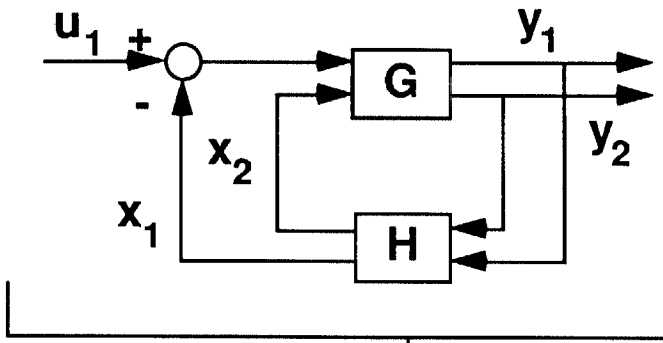

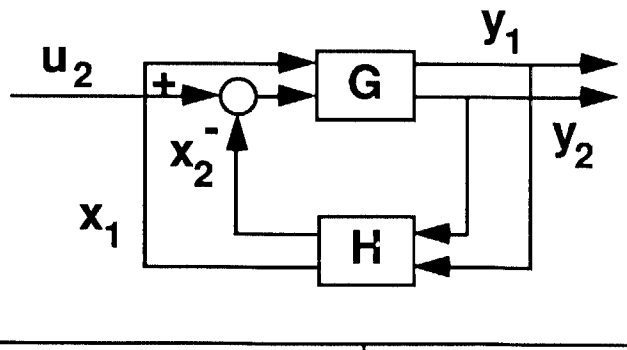

$$Y_u(\omega) = \begin{bmatrix} \frac{Y_1}{U_1} & \frac{Y_1}{U_2} \\ \frac{Y_2}{U_1} & \frac{Y_2}{U_2} \end{bmatrix}$$

$$X_u(\omega) = \begin{bmatrix} \frac{X_1}{U_1} & \frac{X_1}{U_2} \\ \frac{X_2}{U_1} & \frac{X_2}{U_2} \end{bmatrix}$$

COMPUTATION OF PLANT, CONTROLLER AND RETURN DIFFERENCE MATRICES

In order to accomplish the objectives of open- and closed-loop CPE, the plant transfer matrix, controller transfer matrix, and return difference matrices must be determined. This chart outlines how this is accomplished.

Open loop. In the open-loop case, both transfer matrices, $\mathbf{X}_u$ and $\mathbf{Y}_u$, are obtained from a control system in which the loop is open at the controller output. In this case, the plant transfer matrix, **G**, (dimensioned number of sensors by number of actuators, i.e. n_s by n_a) has been directly obtained from the experimental data and is $\mathbf{Y}_u$. The open-loop controller-plant transfer matrix, **HG**, (dimensioned n_a by n_a) is also directly obtained from the experimental data and is $\mathbf{X}_u$.

The controller transfer matrix, **H**, (dimensioned n_a by n_s) is given by the equation shown below the arrow. If n_a is greater than n_s, then this is actually a least square solution.

To perform the first step of the open-loop CPE, the resulting controller transfer matrix, **H**, is compared with the designed control law transfer matrix to verify the implementation of the controller. Specifically, the transfer functions are compared for each output/input pair.

Closed Loop. The difference between closed-loop and open-loop computations is that the transfer matrices, $\mathbf{X}_u$ and $\mathbf{Y}_u$, are obtained from the closed-loop system. During closed-loop testing, the plant transfer matrix is determined from the first equation on the top right side of the figure and the open-loop controller-plant transfer matrix is determined from the second equation. Noting that the quantity,

$$\left[\mathbf{I} - \mathbf{X}_u(\omega)\right]^{-1}$$

is common in both equations, transfer matrices **G** and **HG** are obtained simultaneously using matrix partitioning. The controller transfer matrix, **H**, is calculated the same whether the system is open or closed loop.

The matrix product **GH** is determined by multiplying the two matrices **G** and **H.** The return difference matrices at the plant input (**I+HG**) and at the plant output (**I+GH**) can then be calculated. The significance of these matrices and their singular values, determinants, and eigenvalues will be described next.

COMPUTATION OF PLANT, CONTROLLER AND RETURN DIFFERENCE MATRICES

	OPEN LOOP	CLOSED LOOP
Plant	$G(\omega) = Y_u(\omega)$	$G^T(\omega) = [I - X_u(\omega)]^{-1} Y_u^T(\omega)$
	$HG(\omega) = X_u(\omega)$	$[HG]^T(\omega) = [I - X_u(\omega)]^{-1} X_u^T(\omega)$

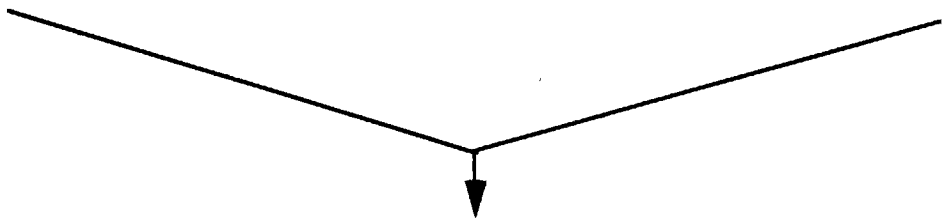

Controller $$H^T = \left[Y_u Y_u^T\right]^{-1} Y_u X_u^T$$

Return difference matrices:

at Plant input	I+HG
at Plant output	I+GH

MEASURE OF STABILITY

DETERMINANT

For MIMO control systems the determinants of the return difference matrices can be used as a direct measure of system stability. Since determinants of the return difference matrix at the plant input and the plant output are identical, only the determinant of one needs to be calculated (the plant input was chosen). The locus of the determinant of the return-difference matrix as a function of frequency has properties similar to those of a Nyquist diagram for SISO control systems. If the open-loop system is stable, an encirclement of the critical point (the origin) for $\det(\mathbf{I}+\mathbf{HG}(\omega))$ indicates that the controller is destabilizing. Furthermore, the proximity of the determinant locus to the critical point is a direct indication of how near to an instability the closed-loop system is. Although Nyquist diagrams for a SISO system can also be used to obtain gain and phase margins, determinant plots cannot provide similar information for MIMO systems. Robustness information for MIMO systems can be obtained from minimum singular values, and how this is obtained is described next.

MEASURE OF STABILITY

DETERMINANT

$$\det (\mathbf{I} + \mathbf{HG})$$

- **Applicable to MIMO control systems**
- **Properties similar to Nyquist diagrams**

MEASURE OF ROBUSTNESS

MINIMUM SINGULAR VALUES

To perform the second step in the open-loop CPE (predicting closed-loop performance based on open-loop information), it is convenient with a MIMO system to evaluate robustness by examining the minimum singular values of the return-difference matrices at the plant input, σ_{min} **(I+HG)** and the plant output , σ_{min} **(I+GH)**.

System instabilities occur when the minimum singular value of the return difference matrix becomes zero. Therefore, the proximity to zero indicates the frequency at which the system is prone to go unstable and provides a quantitative measure of robustness. Reference 3 contains a derivation which relates guaranteed gain and phase margins to minimum singular values. This relationship is shown in the figure, which is a reproduction of figure 2 from reference 3, and will be referred to later when discussing results.

The plot in the lower part of the figure contains information for determining equivalent guaranteed gain and phase stability margins from the minimum singular values of return difference matrices at either the plant input or the plant output. In the figure, the quantity on the ordinate is the minimum singular value; the quantity on the abscissa is gain perturbation, in decibels; the curves are parametric variations in phase perturbation, in degrees. The heavy curve (ϕ=zero degrees) and the heavy vertical line at zero dB have special significance. By using the heavy curve and heavy vertical line, minimum singular values may be "translated" into equivalent guaranteed gain and phase margins (with the conventional SISO interpretations of these margins); by using the parametric curves, minimum singular values may be "translated" into equivalent guaranteed gain and phase margins (with unconventional interpretations of these margins).

The horizontal dashed line in the figure corresponds to a minimum singular value of 0.37. The conventional SISO interpretation of margins is as follows: the intersections of the horizontal dashed line with the heavy curve determines gain margins; the intersection of the horizontal dashed line and the heavy vertical line determines phase margins. Based on these intersections (the right-most, left-most, and center circles), the closed-loop system has guaranteed gain margins of -2.6 dB and +4.0 dB in each loop simultaneously and guaranteed phase margins of +/-22 degrees in each loop simultaneously. The gain margins are understood to be the margins resulting when there is no perturbation in phase introduced into the closed-loop system; the phase margins are understood to be the margins resulting when there is no perturbation in gain introduced into the closed-loop system.

There are an infinite number of unconventional interpretations of these margins. One will be offered and corresponds to the intersections of the horizontal dashed line with the +/-20 degree phase perturbation curve. Based on these intersections (the second and fourth circles), the closed-loop system has guaranteed gain margins of -0.8 dB and +2.1 dB and guaranteed phase margins of +/-20 degrees in each loop simultaneously. That is, within each loop, gain may be varied within these limits (with each loop experiencing a different perturbation in phase), and the closed-loop system is guaranteed to remain stable.

The singular values are a conservative measure of robustness in that a set of gain and phase margins could be constructed that violates the guaranteed margins but fails to destabilize the system. A less conservative measure are the minimum eigenvalues which are described next.

MEASURE OF ROBUSTNESS

MINIMUM SINGULAR VALUES

At the Plant Input:

$\sigma_{min}(I + HG)$

At the Plant Output:

$\sigma_{min}(I + GH)$

Guaranteed Gain and Phase Stability Margins from Minimum Singular Values

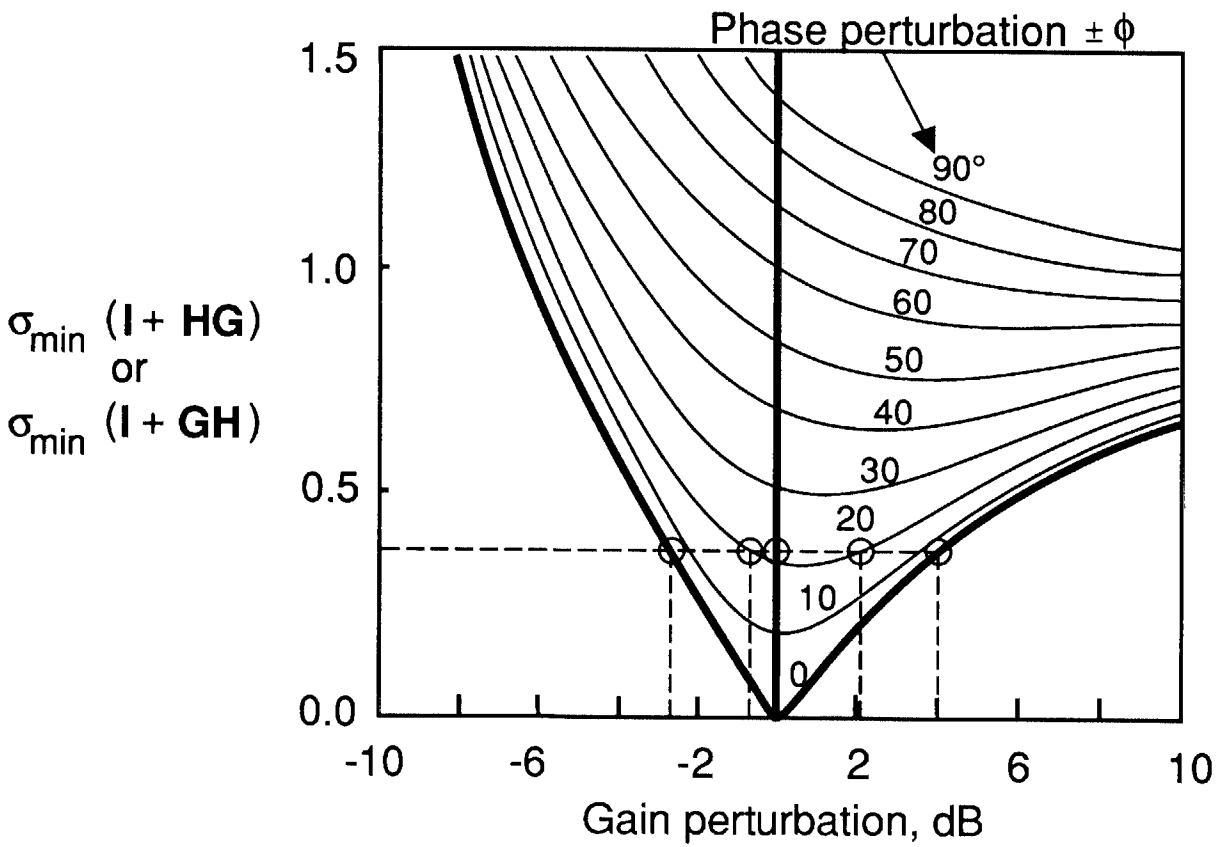

ALTERNATE MEASURE OF ROBUSTNESS

EIGENVALUES

An alternate, and generally less conservative, measure of robustness may be obtained by examining the minimum eigenvalues of the return difference matrices. The minimum eigenvalue at the plant input and the plant output are identical. Therefore, the eigenvalues are only calculated of the return difference matrix at the plant input. In general, the properties of the magnitude of the minimum eigenvalues are similar to the properties of the minimum singular values; both are measures of how close the return-difference matrices are to a singularity.

With minimum eigenvalues now substituted for minimum singular values, the chart from the previous page may be used in an identical manner to obtain gain and phase margins. The interpretation of the margins, however, is different. For a given minimum eigenvalue, in the case of changing the gains by the same amount in all the loops simultaneously without changing phase, the values for the gain margin can be determined from the universal gain and phase margin diagram using the value of the magnitude of the minimum eigenvalue. The same holds true for identical phase changes in all the loops simultaneously with no gain perturbation. These phase and gain changes gives a more realistic indication of the margins than those obtained from minimum singular values.

ALTERNATE MEASURE OF ROBUSTNESS

EIGENVALUES

$$| \lambda_{min}(I + HG) |$$

- Applicable to MIMO control systems
- Less conservative measure of robustness than minimum singular values

IMPLEMENTATION OF CPE METHODOLOGY

This figure shows schematically the hardware used to perform the CPE for the AFW Flutter Suppression System (FSS). Two SUN 3/160 computers were used to conduct Controller Performance Evaluation. The computer identified as SUN-1, not only provided basic control and flutter suppression of the model, but was the source for the excitations needed for CPE. The excitation was generated digitally and added to the control law actuator commands. The digital excitation, actuator commands, and sensor measurements used by the control law were stored and then transferred to SUN-2, equipped with an array processor board. The FFT computations, transfer function calculations and detailed CPE computations were performed on SUN-2.

The FFT's of the time histories of the excitations and the responses, and the transfer functions, were computed by a Fortran-77 program, optimized to take advantage of the vector-processing capabilities on the array processor. The detailed CPE analysis capability was implemented using MATLAB software operations (reference 8). Functions and procedure files were written to perform the matrix computations, eigenvalue analysis, and plot the results.

IMPLEMENTATION OF CPE METHODOLOGY

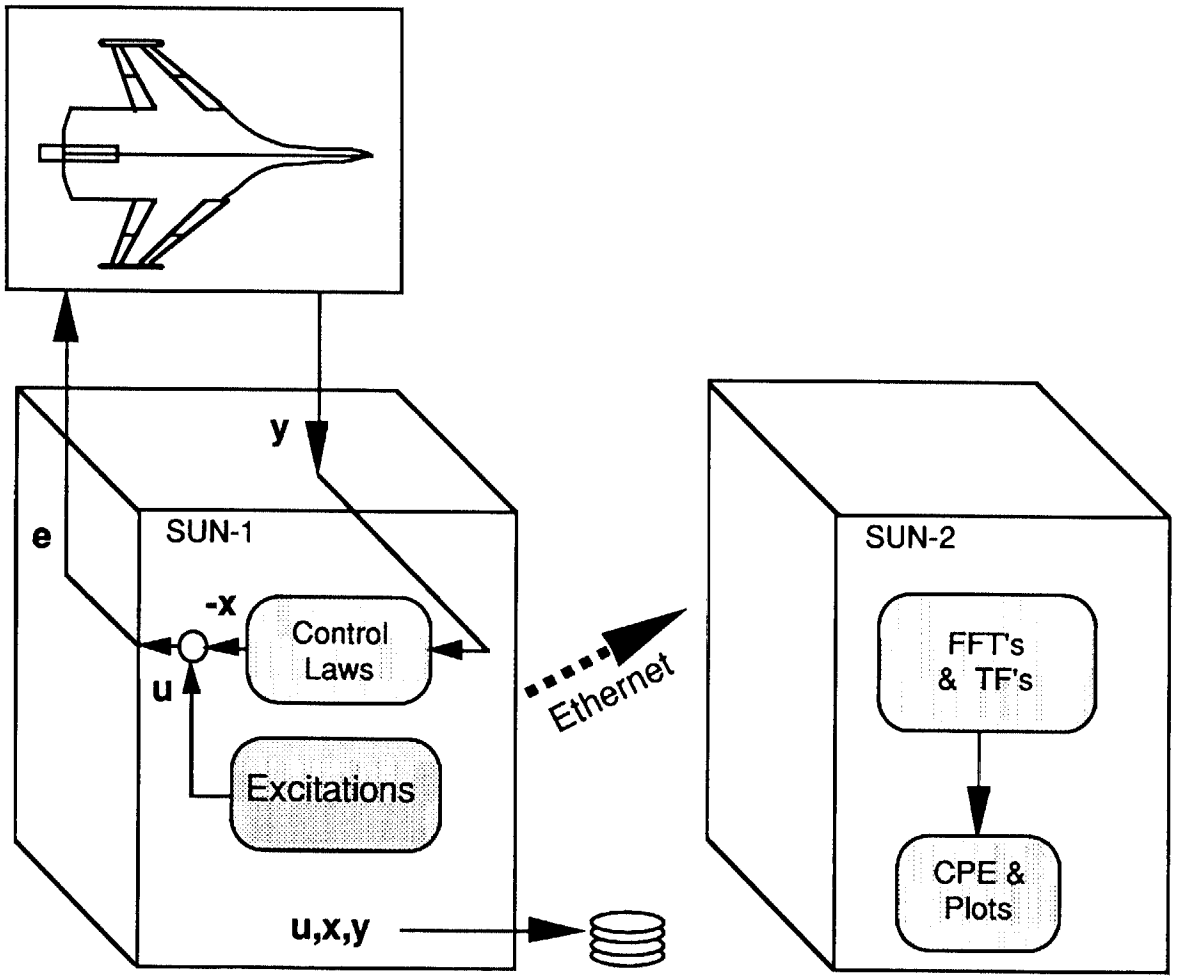

- **Fortran 77 optimized for array processor**
- **Commercially available software package**

OPEN-LOOP CPE RESULTS

EVALUATION POINTS

Wind-tunnel test results will be provided for both open- and closed-loop CPE to demonstrate the objectives which were specified earlier. Both SISO and MIMO flutter suppression control laws were designed for the AFW wind-tunnel model. During the wind-tunnel test the FSS control laws were successfully tested and their closed-loop performance was evaluated using the CPE capability presented in this paper.

Open-loop CPE results are presented first. Shown in the figure is the atmospheric H line along which wind-tunnel testing was conducted. This curve gives the dynamic pressure and Mach number variation as the tunnel fan blade speed is increased when the wind-tunnel total pressure is initially one atmosphere. The two solid circles represent conditions at which open-loop CPE was performed: the first, at a dynamic pressure of 100 psf, corresponds to a stable plant and a stable closed-loop system. The closed-loop system was predicted to be stable and therefore the loop was closed. Closed-loop flutter suppression testing commenced. At a dynamic pressure of approximately 175 psf, below the flutter boundary of 221 psf, the closed-loop system became unstable. The safety mechanisms installed in the model and in the wind tunnel tripped and the dynamic pressure was decreased. The system was then tested open loop and the dynamic pressure was again increased. Open-loop CPE was performed at a dynamic pressure of 175 psf. The results for a dynamic pressure of 100 psf will be presented first followed by the results at 175 psf.

OPEN-LOOP CPE RESULTS

Evaluation Points

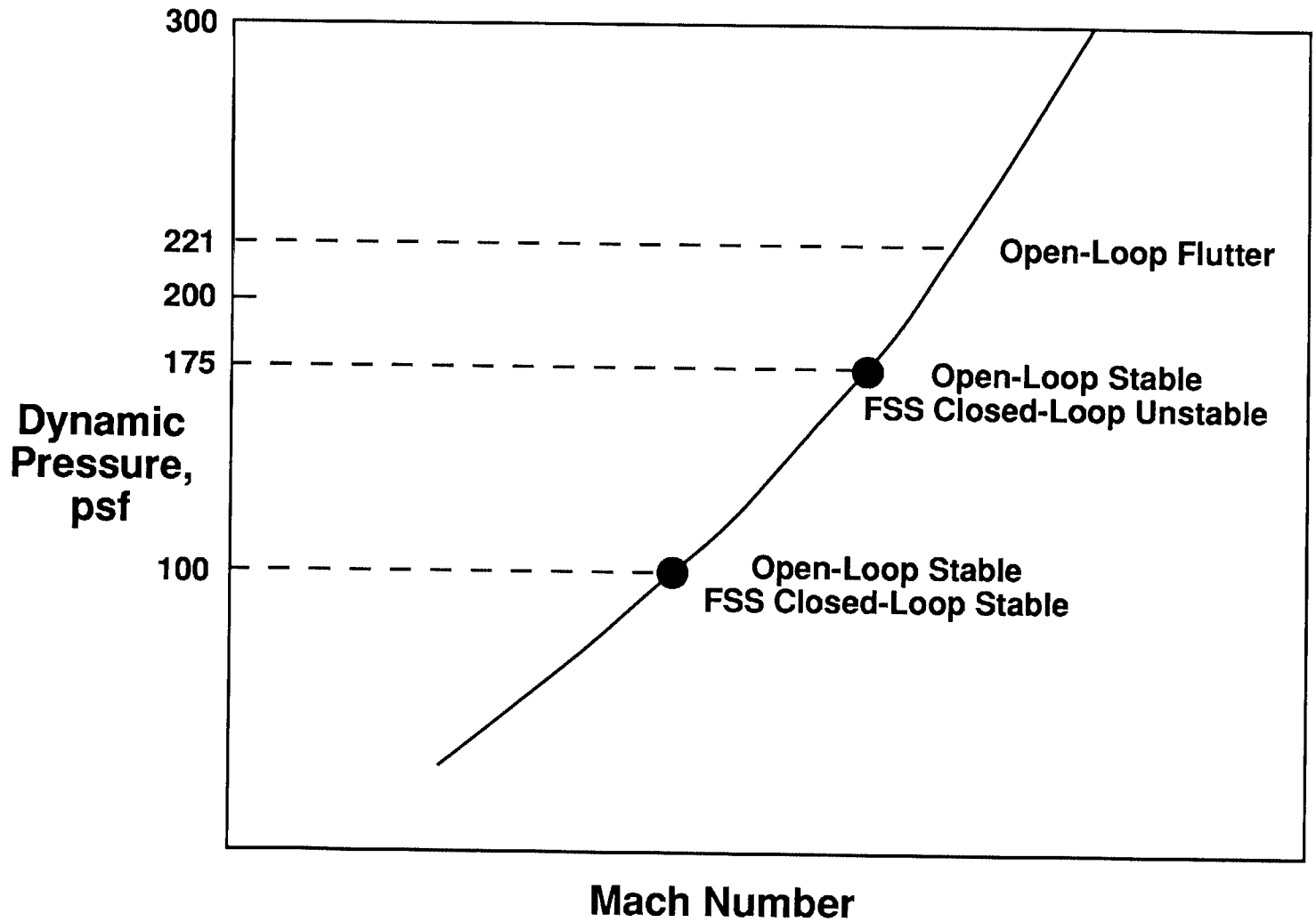

OPEN-LOOP CPE RESULTS

Stable Plant/Stabilizing Controller

This figure contains CPE information exactly the way it comes off the laser printer in the control room during the wind-tunnel test. The CPE results consist of four plots, which together give a complete picture of the performance of the controller. In the upper left hand side are the maximum and the minimum singular values of the return difference matrix at the plant input. On the upper right are the maximum and minimum singular values of the return-difference matrix at the plant output. The lower left shows the magnitudes of the minimum eigenvalue of the return difference matrix. The lower right is the locus of the determinants of the return difference matrix.

This figure corresponds to the first solid circle from the previous figure. During FSS testing, this CPE information is used in the following way: First, the determinant plot in the lower right is examined. Since there are no encirclements about the critical point, the prediction is that the closed-loop system would be stable if the loop were closed. Next the guaranteed gain and phase margins are determined from the minimum of the minimum singular values (which for this case is 0.17) and the universal gain and phase margin diagram. If the loop is closed, the stability margins will consist of simultaneous gain margins of -1.5, 1.5 dB for 0 phase perturbation and 8 degrees of phase margin with 0 dB gain perturbation. A low minimum singular value is observed near a frequency of 20 Hz which is attributed to a control mode. This is a frequency range where one needs to be alert for instability when the loop is closed.

During wind-tunnel testing the loop was closed on the control law and the closed-loop CPE looked very similar. The control surface activity was quite large at a frequency of 20 Hz which was expected.

The dynamic pressure was then increased. An instability was reached at approximately 175 psf which was below the previously measured open-loop flutter boundary at 221 psf. The loop was then opened and open-loop CPE was performed at a dynamic pressure of 175 psf. These results are presented on the next slide.

OPEN-LOOP CPE RESULTS

Stable Plant / Stabilizing Controller

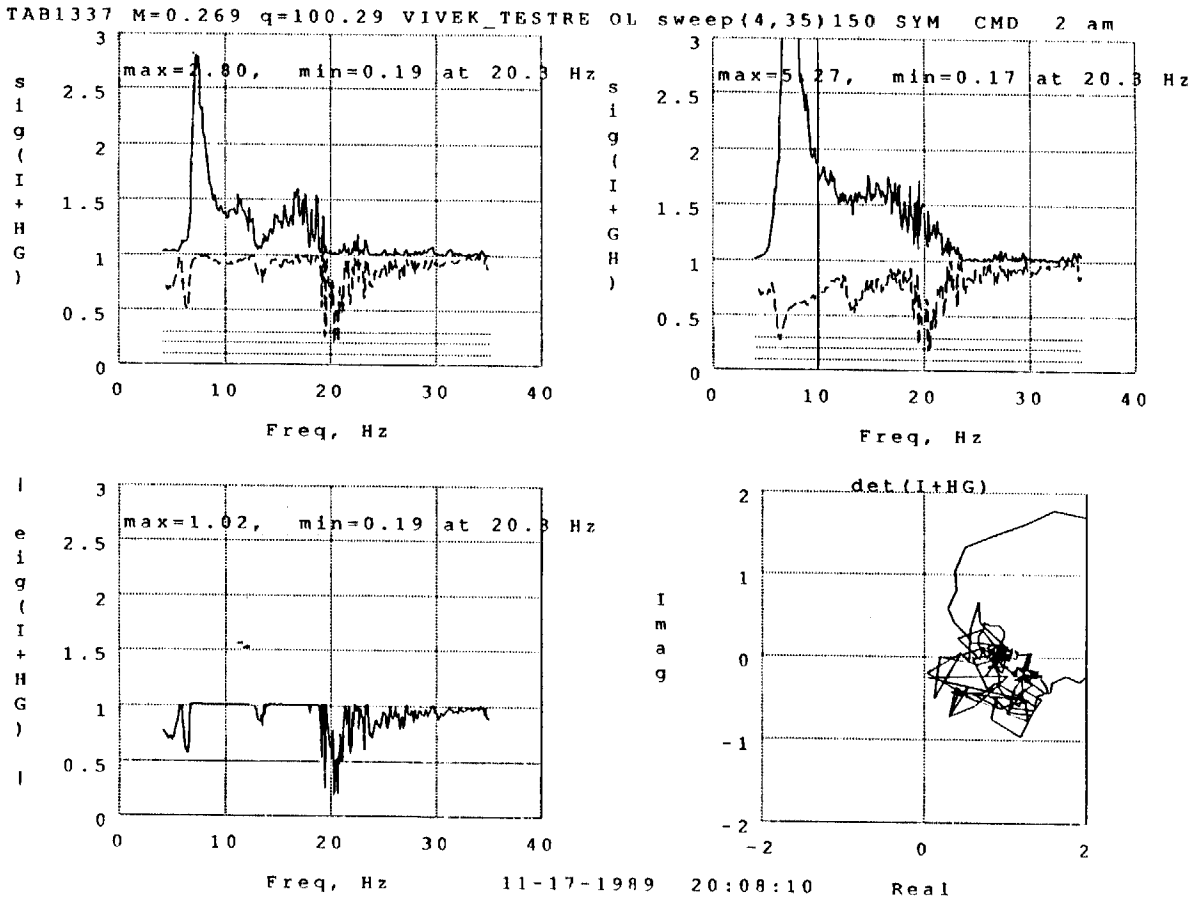

Interpretation: **Closed-loop system stable**

GM= -1.5, 1.5 dB (Phase= 0 deg)

PM= 8 deg (Gain= 0dB)

640

OPEN-LOOP CPE RESULTS

Stable Plant/Destabilizing Controller

This figure contains open-loop CPE results at a condition corresponding to a stable plant and a destabilizing controller. For such a situation, theory predicts that the determinant plot should contain a clockwise encirclement of the origin. The determinant plot (lower right) shows just such an encirclement. This result provided confidence that in the future determinant plots can be used to predict destabilizing control laws.

OPEN-LOOP CPE RESULTS

Stable Plant / Destabilizing Controller

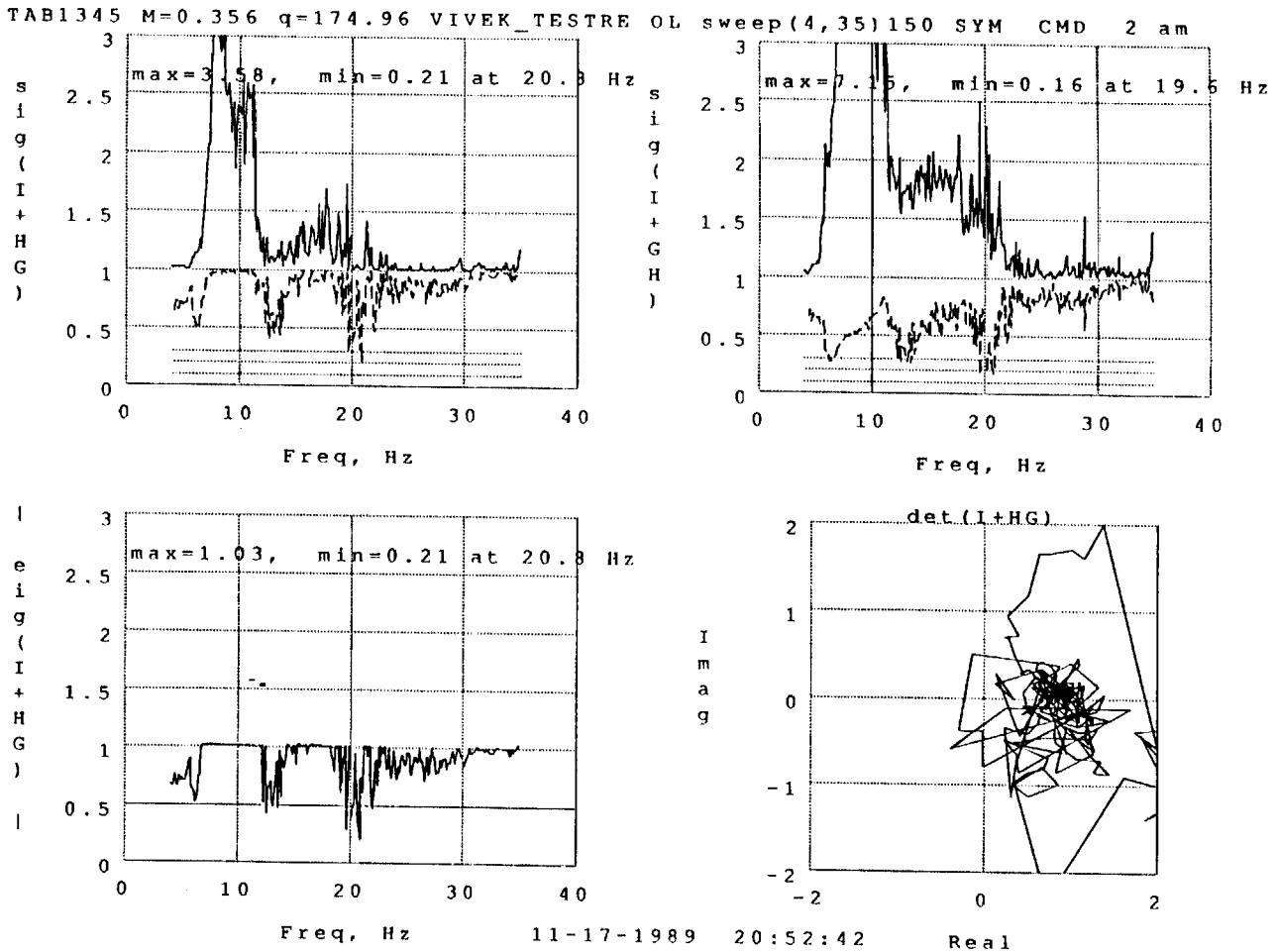

Interpretation: **Closed-loop system unstable**

CLOSED-LOOP CPE RESULTS

Evaluation Points

Typical CPE results obtained during the closed-loop wind-tunnel tests are described next. This figure shows the atmospheric H line along which the wind-tunnel testing was conducted. Two results will be presented. The first is at a point where it is known that the open loop plant was stable and the second where the plant was known to be unstable. The controller was stabilizing for both cases.

CLOSED-LOOP CPE RESULTS

Evaluation Points

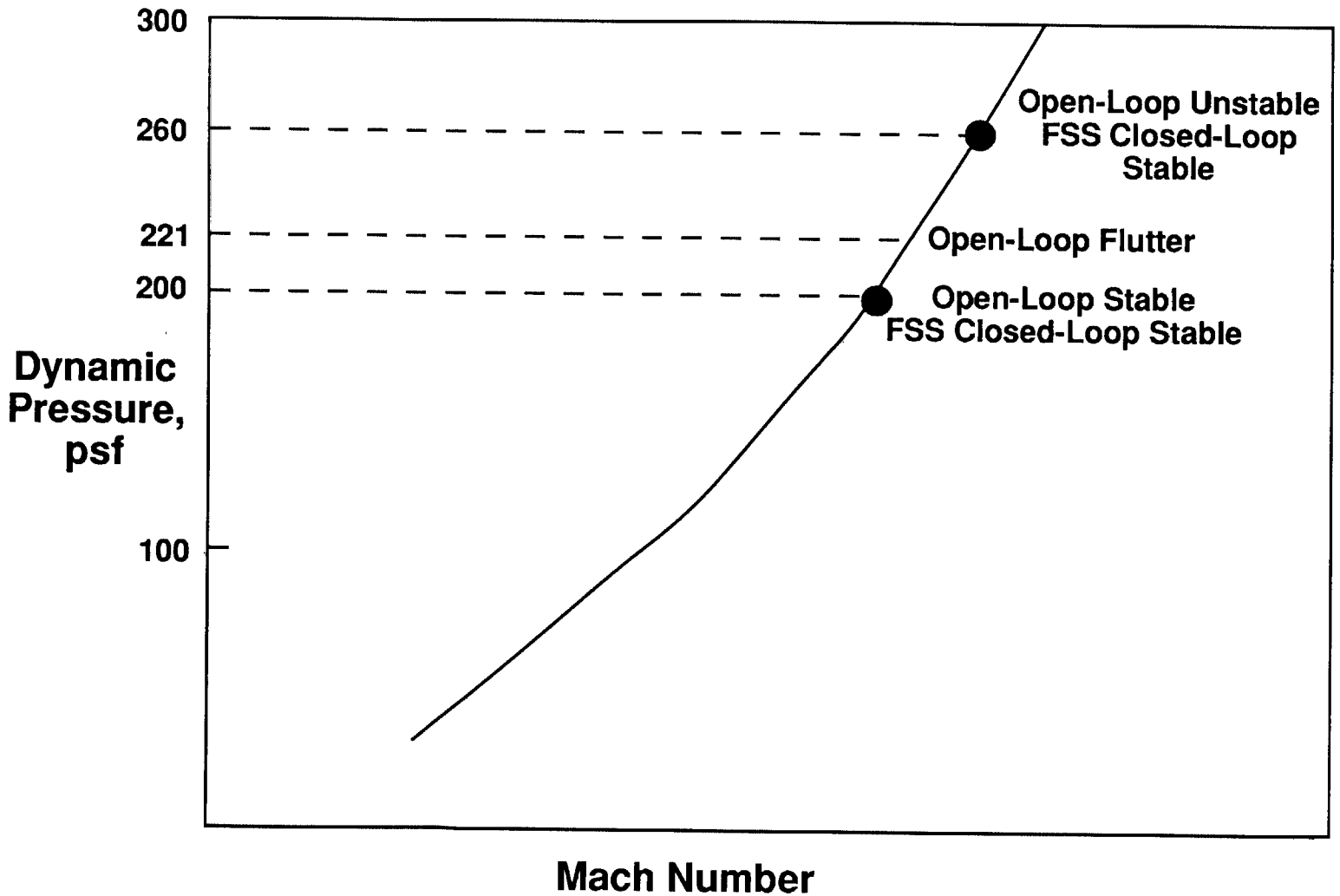

CLOSED-LOOP CPE RESULTS

Stable Plant/Stabilizing Controller

This figure shows the closed-loop CPE results at a dynamic pressure where the plant is known to be stable and the controller is stabilizing. The first objective of closed-loop CPE was to evaluate the stability margins. The guaranteed simultaneous gain and phase margins obtained for a minimum singular value of 0.34 were determined to be -2.6, 3.8 dB gain margin with 0 phase perturbation and 27-degree phase margin with 0 dB gain perturbation. The determinant plot on the bottom right shows no encirclement about the origin (the critical point) which is expected since the plant is stable and the closed-loop system is stable.

The dynamic pressure was then increased to a point above the open-loop flutter boundary, and these results are shown on the next slide.

CLOSED-LOOP CPE RESULTS

Stable Plant / Stabilizing Controller

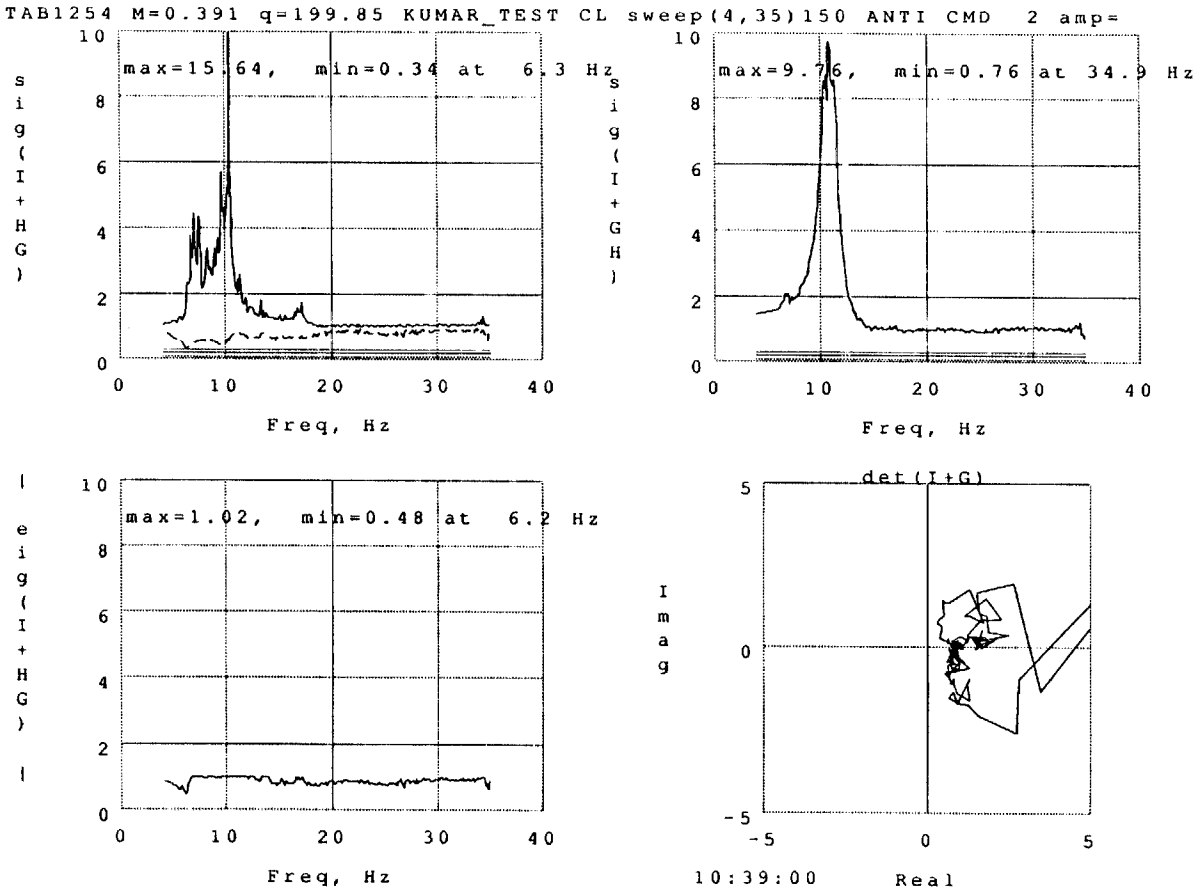

Interpretation { **GM= -2.6, 3.8 dB (Phase= 0 deg)**
PM= 27 deg (Gain= 0dB)

646

CLOSED-LOOP CPE RESULTS

Unstable Plant

The CPE results of a closed-loop system where the plant is known to be unstable and the controller is stabilizing are presented in this figure. Observation of the model in the wind tunnel indicates that the controller is stabilizing the plant so a counterclockwise encirclement about the critical point is expected. The determinant plot shows no clear encirclement. This could be attributed to poor frequency resolution in the region of the encirclement.

Using the minimum singular value of 0.22, the gain margin for 0 phase perturbation are approximately -1.7,+2.1 dB and the phase margin for 0 gain perturbation is ±12.5 degrees.

CLOSED-LOOP CPE RESULTS

Unstable Plant / Stabilizing Controller

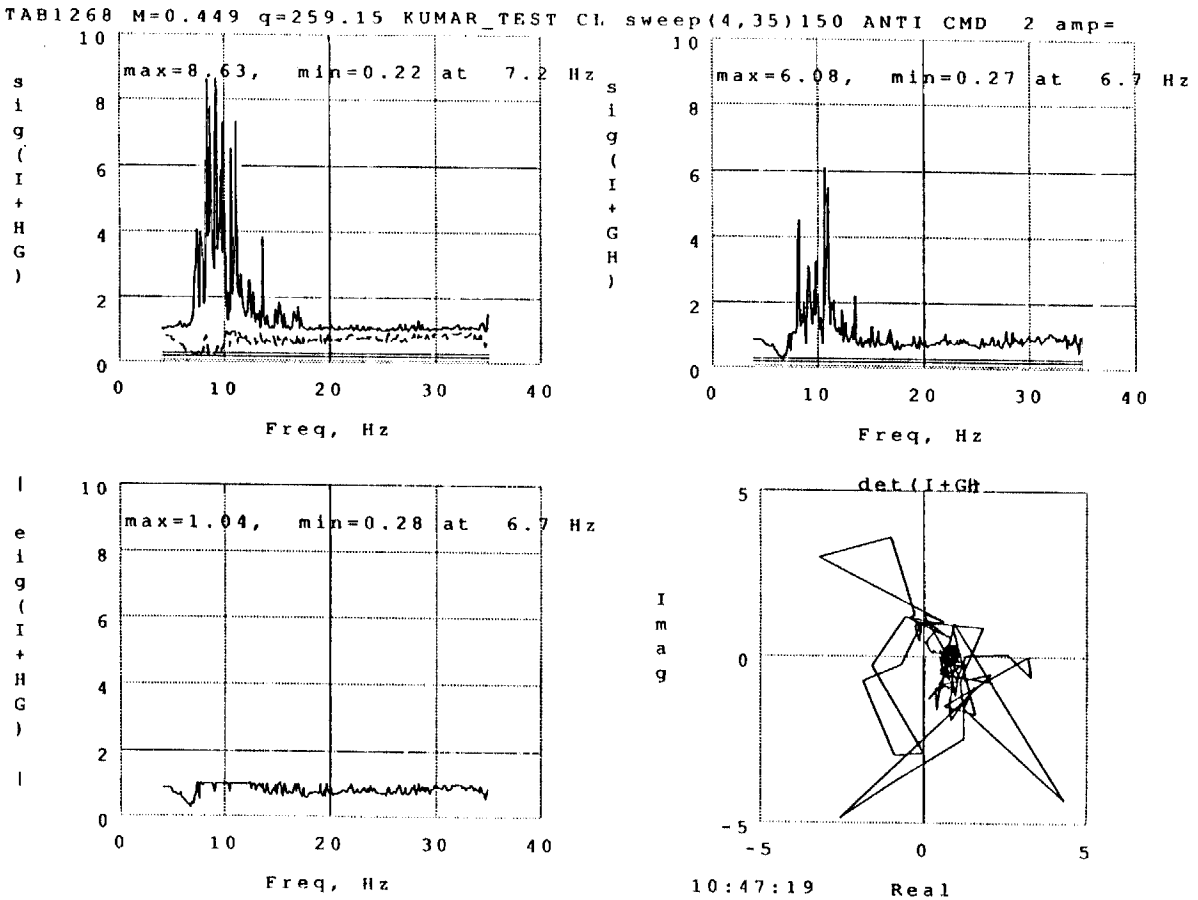

Interpretation { **GM= -1.7, 2.1 dB (Phase= 0 deg)**
PM= 12.5 deg (Gain= 0dB)

FLUTTER PREDICTION PROCEDURE USING CLOSED-LOOP CPE RESULTS

The second objective of the closed-loop CPE was to determine the open-loop stability of the plant during closed-loop testing. The method chosen was based on the observation that poles near the neutral stability axis produce large magnitudes in (SISO) transfer functions. Since maximum singular values of MIMO systems in this respect have similar properties to the SISO transfer functions, then the minimums of the reciprocal of the maximum singular values could be used to indicate how close the the poles of a MIMO system are to being neutrally stable and also the frequencies at which the minimums occur.

During wind-tunnel testing, the plant transfer matrices were obtained during the process of performing closed-loop CPE. A plot of typical inverse maximum singular values of the plant transfer matrix computed from closed-loop tests for a dynamic pressure of 200 psf is shown in the plot on the left. The frequencies (approximately 8.5 and 11 Hz) at which the two local minima of the inverse maximum singular value curve occur are indicated by the arrows. These frequencies correspond to the frequencies of the modes which coalesce to create flutter. These frequencies were determined for many dynamic pressures and the figure on the right shows a plot of the two frequencies as a function of dynamic pressure. The dynamic pressure at which the two curves appear to coalesce indicates a potential point for open-loop flutter.

FLUTTER PREDICTION PROCEDURE USING CLOSED-LOOP CPE RESULTS

650

$$\frac{1}{\sigma_{max}(G)}$$

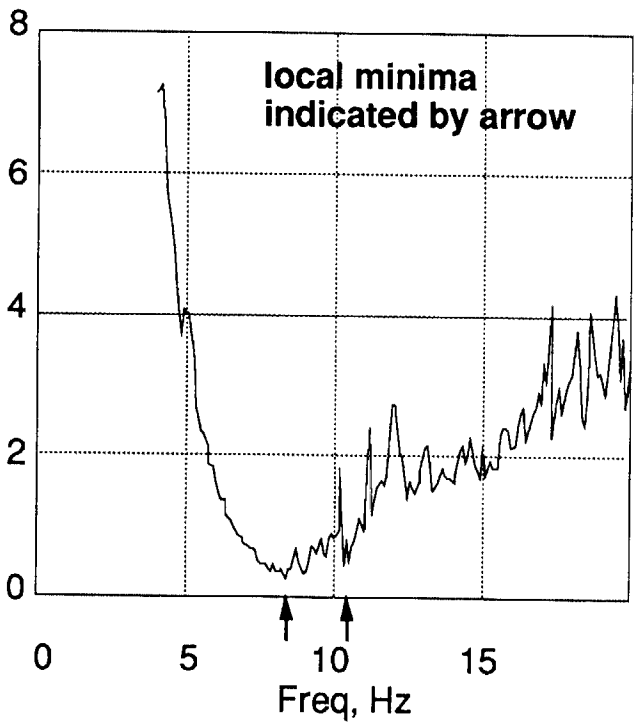

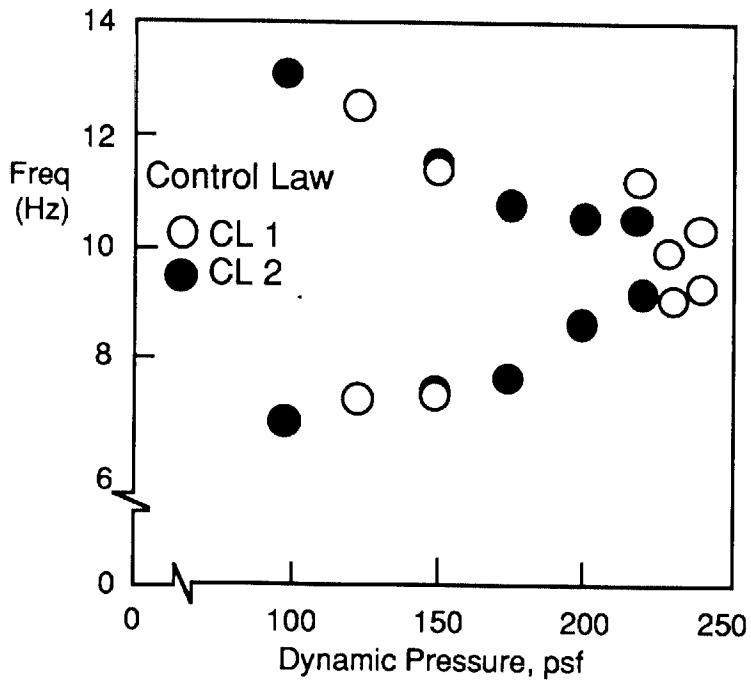

CONCLUDING REMARKS

A Controller Performance Evaluation methodology was developed to evaluate the performance of multivariable, digital control systems. The method was used and subsequently validated during the wind-tunnel testing of an aeroelastic model equipped with a digital flutter suppression controller. Through the CPE effort a wide range of sophisticated near real-time analysis tools were developed. These tools proved extremely useful and worked very well during wind-tunnel testing. Moreover, results from open-loop CPE were the sole criteria for beginning closed-loop testing. In this way, CPE identified potentially destabilizing controllers before actually closing the loop on the control system, thereby avoiding catastrophic damage to either the wind-tunnel model or the wind tunnel. Open-loop plant transfer functions derived from CPE computations were used to redesign and improve control laws. CPE results also proved useful in determining open-loop plant stability during closed-loop test conditions.

CONCLUDING REMARKS

- Developed CPE methodology and tools
- Improved wind-tunnel and model safety
- Sole criteria for closed-loop testing
- Objectives of CPE met
  - Closed-loop system stability predicted from open-loop information
  - Closed-loop stability margins calculated
  - Open-loop plant stability investigated from closed-loop information

REFERENCES

1. Mukhopadhyay, V.; and Newsom, J. R.: A Multiloop System Stability Margin Study Using Matrix Singular Values. *Journal of Guidance, Control, and Dynamics*, Vol. 7 No. 5, September - October 1984, pp. 582-587.

2. Mukhopadhyay, V.; and Newsom, J. R.: Application of Matrix Singular Value Properties for Evaluating Gain and Phase Margins of Multiloop Systems. AIAA Paper 82-1574, AIAA Guidance, Control, and Dynamics Conference, August 9-11, 1982, San Diego, California.

3. Mukhopadhyay, V.; Pototzky, A. S.; and Fox, M. E.: A Scheme for Theoretical and Experimental Evaluation of Multivariable System Stability Robustness. Paper presented at the 1990 American Control Conference, May 23-25, 1990, San Diego, California.

4. Miller, G. D.: Active Flexible Wing (AFW) Technology. AFWAL TR-87-3096, February 1988.

5. Noll, T. E.; et al.: Aeroservoelastic Wind-Tunnel Investigations Using the Active Flexible Wing Model - Status and Recent Accomplishments, NASA TM-101570. AIAA Paper 89-1168, AIAA 30th Structures, Structural Dynamics and Materials Conference, Mobile, Alabama, April 1989.

6. Christhilf, D.; Adams, W. M.; Srinathkumar, S.; Waszak, M.; and Mukhopadhyay, V.: Design and Test of Three Active Flutter Suppression Controllers. 4th Workshop on Computational Control of Flexible Aerospace Systems.

7. Adams, W. M., Jr.; Tiffany, S. H.; and Bardusch, R. E.: Active Suppression of an Apparent Shock Induced Instability, AIAA Paper 87-0881-CP, AIAA 28th Structures, Structural Dynamics, and Materials Conference, April 6-8, 1987, Monterey, California.

8. PRO-MATLAB User's Guide, The MathWorks Inc., 21 Eliot Street, South Natick, MA 01760.